Proceedings of BS2013:
13th Conference of International Building Performance Simulation Association, Chambéry, France, August 26-28

MODELLING OF STREET CANYON GEOMETRIES IN CFD – A COMPARISON WITH EXPERIMENTAL RESULTS

Hui Wen[1], Stella Karra[1], Liora Malki-Epshtein[1]
[1]University College London, London, United Kingdom

ABSTRACT

Street canyon design has a large effect on the microclimate conditions at street level. Yet modeling the outdoor urban environment is a significant challenge and validation with experimental flows is crucial to these efforts. A CFD model was constructed to simulate flow passing several street canyon geometries and the results were compared with those obtained from a laboratory study. The turbulence model chosen was the Re-Normalization Group (RNG) k-ε model which we had found to be a suitable steady state turbulence model for this application. Different inlet boundary conditions were applied and made a comparison between a uniform velocity profile, a velocity profile characterized by a mathematic function and a velocity profile by importing measured velocities directly. The velocity profile characterized by a mathematic function was found to be slightly superior to the other two choices. The velocity fields and turbulence information of the CFD model were compared qualitatively and quantitatively with experimental results. The laboratory experiments were carried out in a water channel and measurements of velocity field within and above models of street canyons were obtained through Particle Image Velocimetry (PIV). Velocity contours were found to be quite consistent inside the street canyon except the near wall regions. Turbulent level predicted by CFD was less reliable than velocity, but it was still qualitatively consistent in most regions inside street canyon. However, the turbulent level is predicted inaccurately at roof level.

INTRODUCTION

Due to increasing traffic volumes in cities, and the associated risks of respiratory disease and asthma, air pollution remains a major environmental concern in urban areas. Certain urban designs, especially street canyons, where a street is flanked by continuous tall buildings on both sides, may lead to accumulation of pollution and generate local pollutant concentrations several times higher than background levels (Karra et al., 2011, Palmgren et al., 1999). Consequently, many studies have been focused on this specific type of urban geometry and its influence on local pollutant distribution. There are three main approaches to study pollutant distribution within street canyons; field measurements, experiment measurements and numerical modelling typically done by CFD (Computational Fluid Dynamics). Field studies can provide direct measurements of pollutant concentrations and wind conditions but usually lack spatial resolution. For example, based on a series of systematic measurements of pollutant and wind conditions in Guangzhou, China, Xie et al. (2003) concluded that a vertical wind vortex would be formed within a street canyon when the angle between the mean wind at roof level and the street was more than 30° and the wind speed was higher than 2m/s. In such case, a significant difference of pollutant concentrations could be found between the windward side and the leeward side. Karra et al. (2011) also found a similar situation in a heterogeneous street canyon. The difference was quite sensitive to the measuring height and measuring location along the street. Experiments are mostly conducted in wind tunnels or water channels in order to obtain detailed flow and pollutant information at reduced scales. Kastner-Klein and Plate (1999) have studied the gaseous pollutant dispersion in street canyon by wind tunnel experiments. They looked at the significance of building dimensions, upwind building arrangement and source position in affecting pollutant distribution inside street canyon. However, experiments are associated with technical difficulties, such as satisfying similarity condition and measuring turbulence information, as well as availability of appropriate wind tunnels and their costs. CFD modelling is relatively economic and time-saving, but its accuracy is highly dependent on the choices of turbulent model, boundary conditions, numerical scheme and other settings. Numerous CFD modelling works have been carried out in this topic. Huang et al. (2009) evaluated the impact of wedge-shape roofs on airflow and pollutant distribution by k-ε model. Cai et al. (2008) used a large eddy simulation (LES) model to study pollutant transportation in several street canyons characterized by different aspect ratio. Gu et al. (2011) also adopted a LES model to study uneven building layout's influence on airflow and pollutant distribution.

We use time-averaged data to qualitatively validate the CFD results by starting from a Reynolds average Navier-Stokes (RANS) model. The CFD data, namely mean velocity and turbulent intensity are compared to experiment measurements. In addition, there has been limited attempt in previous literature to demonstrate the difference between using different inlet profiles. This paper shows the result of simulation using three different inlet boundary profiles.

METHODOLOGY

EXPERIMENT SETTINGS

The experiments were carried out in an open water channel of 0.495m wide, 6.2m long and 0.3m high. The water depth was 0.23m. Rectangular blocks were positioned in the water channel to model flow passing several street canyons, with the first block at 1.916m from inlet. The free-stream velocity at this position is around 0.16m/s. All the blocks were the same size with both width and height 60mm and spanned the width of water channel. The separation distance between each block was fixed as 48mm, which provided an aspect ratio between height to width of the canyons of H/W=1.25. Measurements were taken within and above the third street canyon so as to achieve a more typical urban boundary layer shape before the flow reaches the test street canyon. The velocity profile at 1.7m after the inlet was measured before blocks were added to represent buildings. This profile is later used as an approximate inlet condition in CFD.

Velocity fields were measured by PIV. The laser system was placed vertically on top of the water channel at 0.70m from the bed surface up to the edge of the lens, while the CCD camera was orientated perpendicular to the laser at 0.843m from the glass surface and at 1.57m from the ground level on the right side of the water channel. More details about the techniques and data analysis are presented in Karra (2012).

CFD SIMULATIONS

Geometry

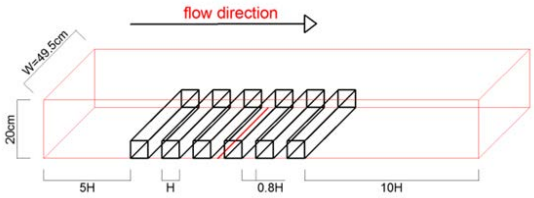

Figure 1 geometry of computational domain

Commercial software ANSYS CFX 12 is used in this CFD simulation. The geometry of experiment was simplified in CFX. The computational domain was extended to 5H between the inflow boundary and the first building, and 10H between the outflow boundary and the last building, where H=60mm is the height and width of the buildings, as recommended by Franke et al. (2007). The depth of water was reduced to 0.2m.

Mesh information

Since the geometry is relatively simple, block-based hexahedral mesh is used to enhance the quality of the mesh. Detailed mesh settings are outlined in Figure 2. All inflation ratios of mesh are kept between 1.1 and 1.2. 18 cells are placed in each building separation, which is higher than the minimum grid resolution 10 cells recommended by Franke et al. (2007). The largest cell size inside the street canyon is 0.053H×0.059H×0.083H. The total number of cells in the entire flow region is around 1 million.

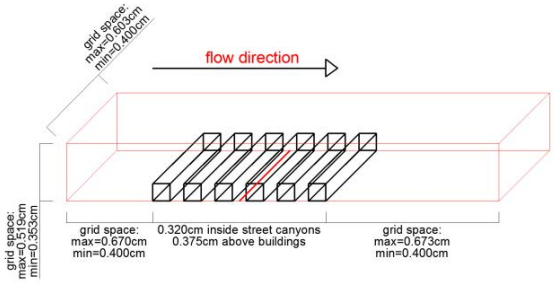

Figure 2 mesh information

Solver control

For terms of advection and turbulent numeric, high resolution schemes were used. In a strict sense, high resolution scheme is a blending strategy between first and second order methods. However, the blending is chosen as close to a second order scheme except in the region where quantities have large gradients that cannot be properly bounded by a second-order scheme (ANSYS, 2010). Hence, it is believed to be second-order accuracy. Convergence target based on root mean square was chosen as 1×10^{-5}. Since CFX is an implicit solver based on a combined finite-volume and finite-element method, pseudo time scale information should be specified for a steady state analysis. We made the solver evaluate the time scale information automatically based on a conservative lengthscale. The time scale was further reduced by a factor of 0.25 to minimize any stability issues during the iteration. Quantities of interest such as velocity and turbulent kinetic energy were monitored at several chosen points during the solving process to ensure they were maintained at stable levels before convergence was met.

RNG k-ε turbulent model for incompressible flow

The renormalization group (RNG) k-ε model was used in this modeling work. It has a similar form as standard k-ε model but with different model constants derived from RNG theory. Moreover, an additional term in the dissipation equation as an *ad hoc* model results in better performance than standard k-ε model in most cases (Pope, 2000).

Kim and Baik (2004) have successfully used RNG k-ε model to investigate the effects of ambient wind direction on flow field and pollutant dispersion in urban areas. Chan et al. (2002) have demonstrated RNG k-ε model to be the most optimum turbulence model relative to standard k-ε model and realizable k-ε model in their case by comparing with the measured and calculated data under different wind speed conditions.

The full governing equations and modeling equations for Reynolds stress and eddy viscosity are shown below.

Continuity equation

$$\frac{\partial U_j}{\partial x_j} = 0 \quad (1)$$

Momentum equation

$$\frac{\partial U_j}{\partial t} + U_j \frac{\partial U_i}{\partial x_j} = -\frac{1}{\rho}\frac{\partial p'}{\partial x_i} + \frac{\mu}{\rho}\frac{\partial^2 U_i}{\partial x_j \partial x_j} - \frac{\partial}{\partial x_j}\overline{u_i' u_j'} \quad (2)$$

Turbulent kinetic energy (k) transport equation

$$\frac{\partial k}{\partial t} + U_j \frac{\partial k}{\partial x_j} = \frac{1}{\rho}\frac{\partial}{\partial x_j}\left[\left(\mu + \frac{\mu_t}{\sigma_{k,RNG}}\right)\frac{\partial k}{\partial x_j}\right] + \frac{\mu}{\rho}\frac{\partial^2 U_i}{\partial x_j \partial x_j} + \mathcal{P}_k - \varepsilon \quad (3)$$

Dissipation (ε) transport equation

$$\frac{\partial \varepsilon}{\partial t} + U_j \frac{\partial \varepsilon}{\partial x_j} = \frac{1}{\rho}\frac{\partial}{\partial x_j}\left[\left(\mu + \frac{\mu_t}{\sigma_{\varepsilon,RNG}}\right)\frac{\partial \varepsilon}{\partial x_j}\right] + \frac{\varepsilon}{\rho k}\left(C_{\varepsilon 1,RNG}\mathcal{P}_k - C_{\varepsilon 2,RNG}\rho\varepsilon\right) \quad (4)$$

Reynolds stress is modeled by Boussinesq hypothesis (or turbulent-viscosity hypothesis).

$$\overline{u_i' u_j'} = -\frac{1}{\rho}\mu_t\left(\frac{\partial U_i}{\partial x_j} + \frac{\partial U_j}{\partial x_i}\right) + \frac{2}{3}k\delta_{ij} \quad (5)$$

Turbulent viscosity is defined as the following equation.

$$\mu_T = \rho C_{\mu,RNG} k^2/\varepsilon \quad (6)$$

P_k is the turbulence production due to viscous force, which is modeled by equation 7. For incompressible flow, the contribution from the second term on the right hand side in equation 7 is negligible (Pope, 2000).

$$\mathcal{P}_k = \mu_t\left(\frac{\partial U_i}{\partial x_j} + \frac{\partial U_j}{\partial x_i}\right)\frac{\partial U_j}{\partial x_j} - \frac{2}{3}\frac{\partial U_k}{\partial x_k}\left(3\mu_t\frac{\partial U_k}{\partial x_k} + \rho k\right) \quad (7)$$

The eight model constants are given in Table 1.

Table 1

Model constants of RNG k-ε model in CFX

$C_{\mu,RNG}$	$C_{\varepsilon 1,RNG}$	$C_{\varepsilon 2,RNG}$	$\sigma_{k,RNG}$
0.085	$1.42 - f_\eta$	1.68	0.7179
$\sigma_{\varepsilon,RNG}$	f_η	η	β_{RNG}
0.7179	$\frac{\eta\left(1-\frac{\eta}{4.38}\right)}{1+\beta_{RNG}\eta^3}$	$\sqrt{\frac{\mathcal{P}_k}{\rho\varepsilon C_{\mu,RNG}}}$	0.012

Boundary conditions

Inflow

Inlet boundary condition in CFX is used at our inlet. We believe that uncertainty from boundary conditions is mainly sourced from inlet because the parameters at the rest of boundaries such as the walls and the outlet are fixed. Therefore, an investigation on the significance of different vertical profiles for inlet velocity was carried out first.

Option 1:

Uniform velocity profile at inlet, U=0.1564m/s, is calculated from an equivalent area-averaged velocity to maintain the same flow rate as the experiment. Inlet velocity is assumed to have a normal component only.

$$\overline{U} = \frac{1}{\delta}\int_0^\delta \langle U\rangle dy \quad (8)$$

An approximate integration via trapezoid method is used to integrate discrete velocity data. Due to each measuring point in experiment is very close, the integration has a good approximation.

Turbulence information is set as medium turbulent intensity (5%) with lengthscale as 0.285m. This is the most robust approach to specify turbulent information on inlet if detailed turbulence information is not available.

If we choose mean velocity as reference velocity, it results the Reynolds number around 7,200 (defined by $Re=U_{ref}H/\nu$). It is higher than the critical Reynolds number 3,400 suggested by Hoydysh et al. (1974) for similarity, so the flow behavior will not be sensitive to slightly different settings between the experiment and the CFD model.

Option 2:

The mean velocity profile is derived from our experiment measurement through a weighted least-square fitting process. The profile comprises of a viscous sublayer (equation 9a) in which the velocity is characterized by a linear relation and a log region (equation 9b) in which the velocity follows log-law. y^+ is the distance from wall (y) normalized by the viscous lengthscale (δ_v), and the demarcation of these two regions is set at y^+=12. We use the same turbulent kinetic energy profile (equation 10) as Salim et al. (2011). The dissipation profile (equation 11) is derived from a wall-bounded turbulent flow (see chapter 10.4 of Pope's Turbulent Flow). To avoid infinite dissipation near wall, δ_v is added in the denominator.

$$U = \frac{\rho y U^{*2}}{\nu}, if\ y^+ \le 12 \quad (9a)$$

$$U = \frac{U^*}{\kappa}\ln\frac{y}{z_0}, if\ y^+ > 12 \quad (9b)$$

$$k = \frac{{U_\tau}^2}{\sqrt{C_\mu}}\left(1 - \frac{y}{0.2}\right) \quad (10)$$

$$\varepsilon = \frac{{U_\tau}^3}{\kappa(y+\delta_v)} \quad (11)$$

U_τ is the friction velocity 0.012m/s derived from our experiment in the lower region of channel (under 30% of water depth). U* is a pseudo friction velocity 0.010m/s used to maintain the mass flow rate of velocity profile same as the uniform velocity option and velocity profile determined by functions. Z_0 is 1.32×10^{-3}m as one of fitting parameters. δ_v is viscous lengthscale 1.10×10^{-4}m calculated from derived friction velocity.

Option 3:

Import velocity data from experimental measurements directly, and the profile is built by interpolation function in CFX. Turbulent kinetic energy and dissipation profiles are identical to option 2.

Outflow

Outlet condition with 0Pa static pressure with respect to the reference pressure is applied to force the flow to come out in the direction normal to the outlet without any backflow.

Free surface for the open channel flow

A free-slip wall condition is employed to model the free surface. Free-slip condition is characterized by zero shear stress which matches the real condition exactly. However, this treatment fails to capture wave components since "near-wall" velocity is forced to be parallel to the virtual upper boundary. This boundary condition has been successfully applied in many open channel flow analyses. (Beaman, 2010, Thomas and Williams, 1995). It is a reasonable approximation in our case as we are interested in the street canyon region which is in a deep layer of the flow.

Bottom of channel

Smooth wall with no-slip condition is applied.

Side walls

Smooth wall with no-slip condition is applied.

RESULTS AND DISCUSSION

Cut plane

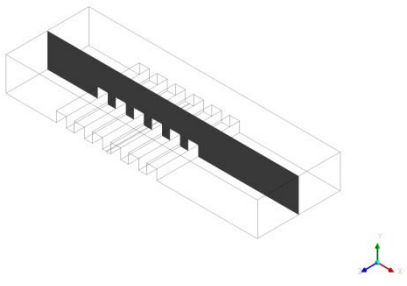

Figure 3 Cut plane in the middle of flow channel

A cut plane perpendicular to spanwise direction is shown in the middle of the channel to display the results (Figure 3). It should be noted that all the analyses are based on quasi-steady state assumption, and experiment results were collected on a time-average base after the flow had become relatively steady.

(a)

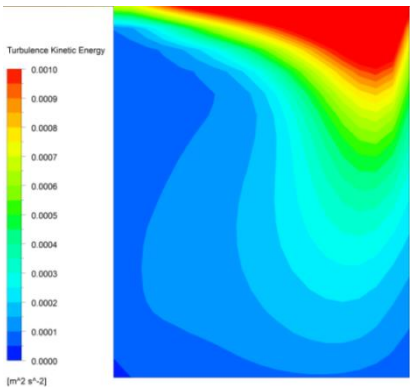

(b)

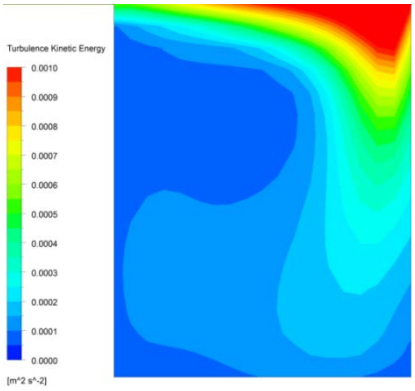

(c)

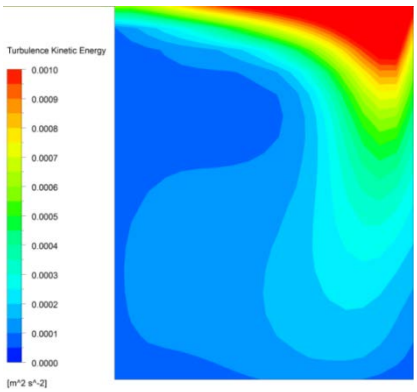

Figure 4 TKE contours for the 3rd street canyon. (a) inlet option 1(b) inlet option 2 (c) inlet option 3

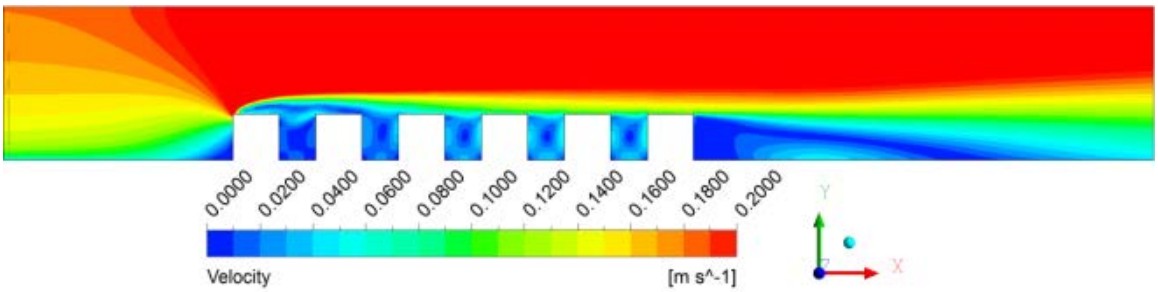

Figure 5 velocity contour for the whole flow domain-CFD results

Table 2

Area-averaged velocity at cut plane corresponding to different inlet options

Inlet option	1	2	3
Area-averaged velocity	2.13×10^{-2} m/s	2.61×10^{-2} m/s	2.55×10^{-2} m/s

Table 3

Area-averaged turbulent kinetic energy (TKE) at cut plane corresponding to different inlet options

Inlet option	1	2	3
Area-averaged TKE	2.97×10^{-4} m^2/s^2	2.27×10^{-4} m^2/s^2	2.50×10^{-4} m^2/s^2

Significance of different inlet options

The overall velocity and turbulent kinetic energy inside the test street canyon could be affected by different inlet condition options. The difference is not very large, as indicated by the contours. For example, Figure 4(a) to 4(c) reveals that constant velocity inlet boundary leads higher turbulent kinetic energy at the center and the upper part of leeward side of the 3rd street canyon than other two inlet options. The difference of turbulent kinetic energy between option 2 and option 3 is not noticeable from the figures. However, when these quantities are presented in a statistical form such as area-averaged quantities, the significance of the different quantities is more apparent. Table 2 reveals that area-averaged velocity can show variations as high as 20% between the different options. A similar situation is also found for turbulent kinetic energy (Table 3). The area-averaged velocity obtained from experiment is 0.0336m/s, which is higher than all three options. The under-prediction by CFD is also apparent after comparing Figure 6 and Figure 7. We hope this under-prediction trend can be minimized. Therefore, we choose option 2 as a conventional approach which is more physically consistent compared to option 1 and more robust compared to option 3.

Mean flow field

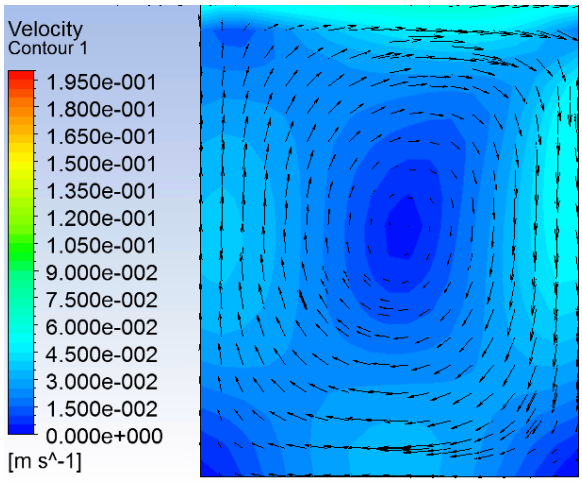

Figure 6 velocity contour for the 3rd street canyon-CFD results

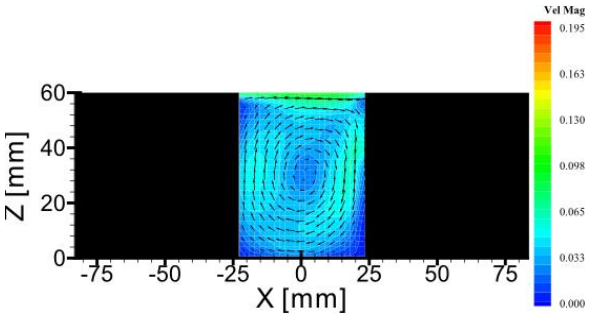

Figure 7 velocity contour for the 3rd street canyon-experiment measurement

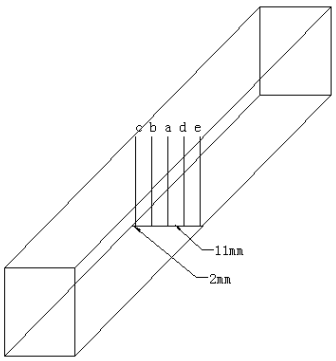

Figure 8 Schematic diagram of 5 chosen locations in Figure 9

(a)

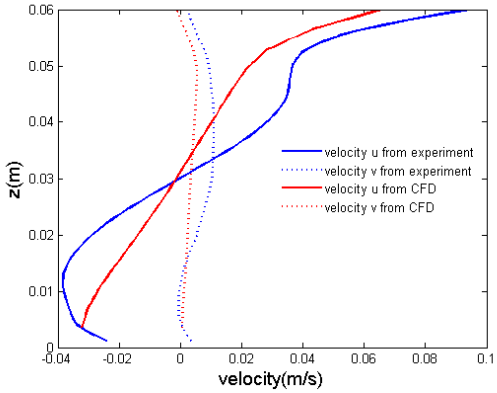

(b)

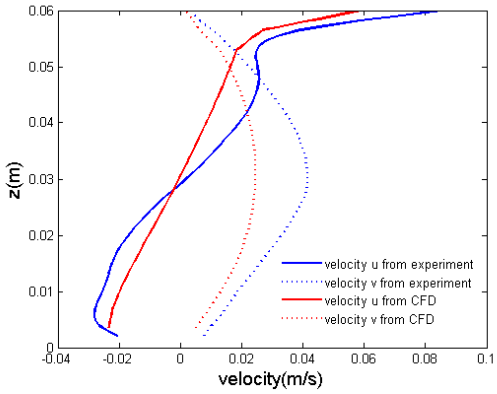

(c)

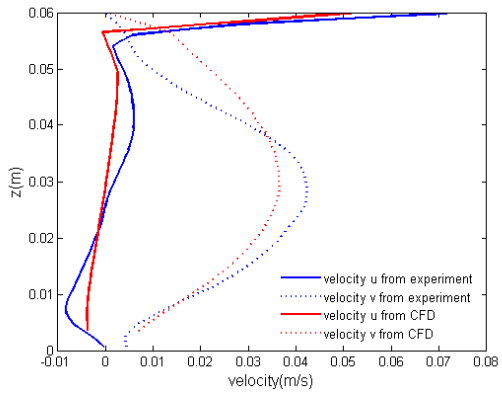

(d)

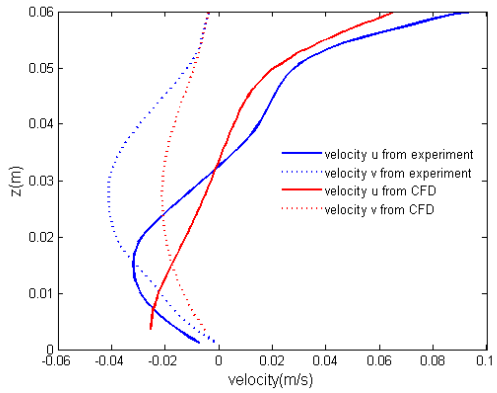

(e)

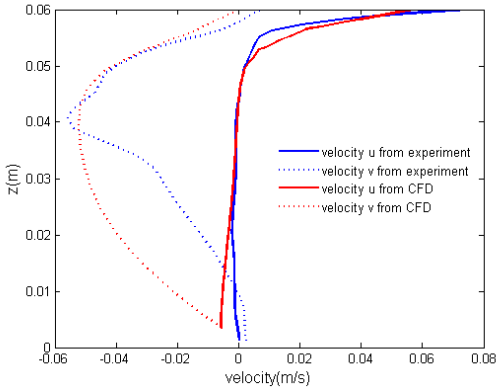

Figure 9 comparisons of velocity components along height between experiment measurement and CFD results. (a) in the middle of cut plane (b) 0.011m left from middle (c) 0.022m left from middle (d) 0.011m right from middle (e) 0.022m right from middle

Figure 6 illustrates velocity magnitude and direction within the third street canyon modeled by CFD. Area-averaged velocity within it is as low as 0.026m/s, compared to the mean velocity at inlet 0.1564m/s. The low velocity inside all of street canyons can be easily observed in Figure 5. Clockwise flow pattern is clearly reflected by the arrows in Figure 6. Even lower speed regions or almost stagnation regions can be observed at the center of plane, two bottom corners and leeward top corner of the test street canyon.

Compared to the velocities measured in experiment (Figure 7), the flow pattern and velocities predicted by CFD are qualitatively consistent with experiment. However, from a quantitative view, CFD under-predicts velocity magnitude in most regions inside the test street canyon. Disparity of velocity components along height between experiment and CFD can be easily discerned in five chosen locations (Figure 9(a) to 9(e)). In detail, vertical velocity component is under-predicted by CFD in all the chosen locations except Figure 5(e). However, since that location is very close to the wall, the reliability of CFD result should be lower than the remote region, due to the result being modeled by the wall function than the solution solved from the governing equations. For horizontal velocity component, CFD seems to under-predict in the lower part but over-predict in the upper part. In addition, velocity gradients are under-predicted by CFD.

Qualitatively, different velocity fields should directly affect pollutant dispersion performance. Lower velocity magnitude attenuates the advection effect by mean flow. Lower velocity gradient gives rise to lower shear rate and Reynolds stress, hence weaker turbulent transport effect.

Furthermore, CFD results suggest that two velocity components are simultaneously close to zero at the location a bit above the geometry center (Figure 9(a)).

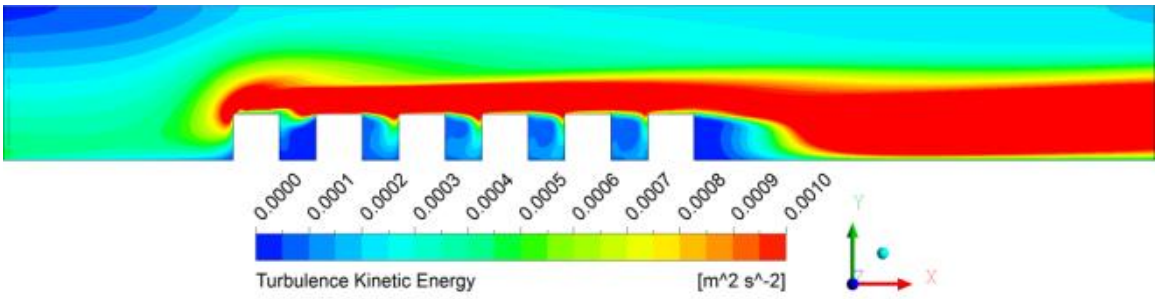

Figure 10 TKE contour for the whole flow domain-CFD results

According to Figure 6 and Figure 7, we could regard the vortex center matches the geometry center in both CFD and experiment. However, the velocity components at vortex center in experiment are non-zero compared to CFD results (Figure 7 and 9(a)). It implies that in real case, the shape of vortex dynamically changes. Vortex center meanders with time, and after making time-average, we get averaged vortex center and these corresponding non-zero velocity components. This fluctuation behavior is unpredictable in RANS model.

Turbulent kinetic energy (TKE) profile

Accurate prediction of turbulent kinetic energy is even more difficult due to the error from model itself and computing procedure (Guillas et al., 2012). Figure 10 reveals that turbulent kinetic energy predicted by CFD within street canyon is almost an order lower than turbulent kinetic energy in the mean flow. One exceptional position is near-roof level especially near windward side, where turbulent kinetic energy is comparable to the mean flow level.

Though turbulent kinetic energy is not the only quantity dominating turbulent transport behavior, we still expect to acquire an acceptable turbulent kinetic energy contour predicted by CFD.

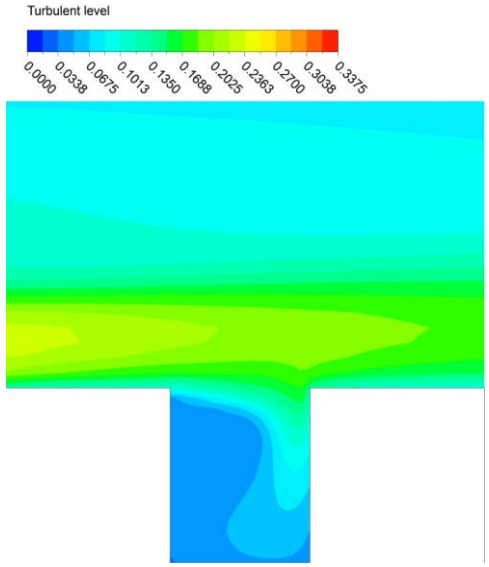

Figure 11Turbulent level contour for the whole flow domain-CFD results

Since the experiment result was obtained on a turbulent level (definition given by equation 12) basis, we convert turbulent kinetic energy to that quantity and then make a comparison.

$$Tl = \frac{\sqrt{\frac{2}{3}k}}{U_{ref}} = \sqrt{\frac{\frac{2}{3}k}{0.1814^2+0.0005^2}} \qquad (12)$$

Figure 11 and Figure 12 indicate that the turbulent levels are comparable inside the test street canyon. Within the street canyon, the most significant under-prediction occurs at the leeward side, center and windward corner. However, the roof level turbulent level is greatly under-predicted by CFD. The shear layer predicted by CFD is much thinner than real thickness indicated by experiment result. Therefore, less turbulent kinetic energy could be transported into street canyon region. However, we could not clarify the under-prediction of turbulent kinetic energy inside street canyon is mainly caused by inaccuracy stem from the local turbulence generation or the turbulence transported from roof level.

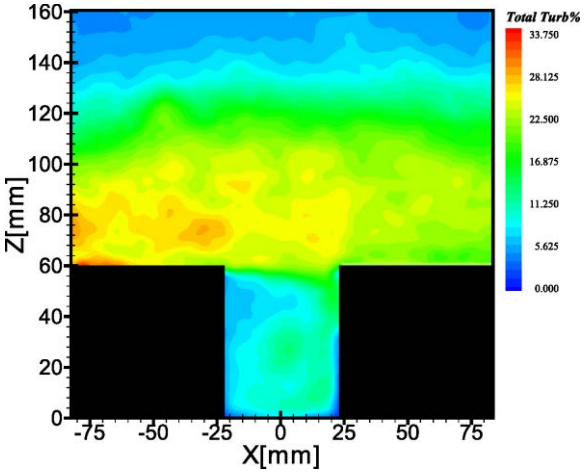

Figure 12 Turbulent level contour for the whole flow domain-experiment results

CONCLUSION

In this study, a comparison between CFD simulation done by RNG k-ε model and experiment measurements have been carried out, aiming to study flow pattern within an ideal symmetrical street canyon. Three main findings can be concluded.

Different inlet conditions have a limited effect on the flow quantities inside street canyon. The differences are more clearly indicated by area-averaged quantities than contours. Using an expression for the velocity profile as well as turbulent kinetic energy and disspation profiles is a more robust and consistent apporach than setting a constant velocity or than directly importing experimental data. The effect that the choice of inlet proflie has on the area-averaged velocity and turbulent kinetic energy are up to 20%.

The velocities inside the street canyon are under-predicted by CFD in most regions of the street canyon except for the common occurrence of over-prediction of horizontal velocity component at the upper part of the leewarde side. Moreover, the velocity gradient is universally under-predicted by CFD. Therefore, we expect weaker advection effect and turbulent transport effect in our CFD model than in reality.

The predicted turbulent kinetic energy is less reliable than the predictions of velocity, because of the limitation of turbulent model itself. CFD under-predicts turbulent kinetic energy both inside and above street canyon. Furthermore, the shear layer above the roof is much thinner than the real thickness indicated by experiment results. Less turbulence is generated at roof level, and hence less turbulent kinetic energy can be tranported into the street canyon region. It is consistent with the under-prediciton of turbulent kinetic energy inside street canyon, but the root cause of under-prediction is not clear yet.

REFERENCES

ANSYS, I. 2010. ANSYS CFX-Solver Theory Guide. U.S.A.: ANSYS, Inc.

BEAMAN, F. 2010. *Largy eddy simulation of open channel flows for conveyance estimation.* Doctor of Philosophy, University of Nottingham.

CAI, X. M., BARLOW, J. F. & BELCHER, S. E. 2008. Dispersion and transfer of passive scalars in and above street canyons—Large-eddy simulations. *Atmospheric Environment,* 42**,** 5885-5895.

CHAN, T. L., DONG, G., LEUNG, C. W., CHEUNG, C. S. & HUNG, W. T. 2002. Validation of a two-dimensional pollutant dispersion model in an isolated street canyon. *Atmospheric Environment,* 36**,** 861-872.

FRANKE, J., HELLSTEN, A., SCHLÜNZEN, H. & CARISSIMO, B. 2007. *Best practice guideline for the CFD simulation of flows in the urban environment,* COST Office.

GU, Z.-L., ZHANG, Y.-W., CHENG, Y. & LEE, S.-C. 2011. Effect of uneven building layout on air flow and pollutant dispersion in non-uniform street canyons. *Building and Environment,* 46**,** 2657-2665.

GUILLAS, S., GLOVER, N. & MALKI-EPSHTEIN, L. 2012. Spatial statistical calibration of CFD modelling of street canyons flows. *5th International Building Physics Conference.* Kyoto, Japan.

HOYDYSH, W. G., GRIFFITHS, R. A. & OGAWA, Y. 1974. A scale model study of the dispersion of pollutant in street canyons. *67th annual meeting of the air pollution control association.* Denver, CO.

HUANG, Y., HU, X. & ZENG, N. 2009. Impact of wedge-shaped roofs on airflow and pollutant dispersion inside urban street canyons. *Building and Environment,* 44**,** 2335-2347.

KARRA, S. 2012. *An investigation of traffic related pollutants dispersion in heterogeneous street canyon.* Doctor of Philosophy, University College London.

KARRA, S., MALKI-EPSHTEIN, L. & NEOPHYTOU, M. 2011. The Dispersion of Traffic Related Pollutants Across a Non-Homogeneous Street Canyon. *Procedia Environmental Sciences,* 4**,** 25-34.

KASTNER-KLEIN, P. & PLATE, E. J. 1999. Wind-tunnel study of concentration fields in street canyons. *Atmospheric Environment,* 33**,** 3973-3979.

KIM, J.-J. & BAIK, J.-J. 2004. A numerical study of the effects of ambient wind direction on flow and dispersion in urban street canyons using the RNG k–ε turbulence model. *Atmospheric Environment,* 38**,** 3039-3048.

PALMGREN, F., BERKOWICZ, R., ZIV, A. & HERTEL, O. 1999. Actual car fleet emissions estimated from urban air quality measurements and street pollution models. *Science of The Total Environment,* 235**,** 101-109.

POPE, S. B. 2000. *Turbulent Flows,* Cambridge, Cambridge University Press.

SALIM, S. M., CHEAH, S. C. & CHAN, A. 2011. Numerical simulation of dispersion in urban street canyons with avenue-like tree plantings: Comparison between RANS and LES. *Building and Environment,* 46**,** 1735-1746.

THOMAS, T. G. & WILLIAMS, J. 1995. Large eddy simulation of symmetric trapezoidal channel at Reynolds number of 430,000. *Journal of Hydraulic Research,* 33**,** 825-842.

XIE, S., ZHANG, Y., QI, L. & TANG, X. 2003. Spatial distribution of traffic-related pollutant concentrations in street canyons. *Atmospheric Environment,* 37**,** 3213-3224.